AFRL-RQ-WP-TP-2017-0169

ANALYSIS OF WINDWARD SIDE HYPERSONIC BOUNDARY LAYER TRANSITION ON BLUNTED CONES AT ANGLE OF ATTACK

Roger L. Kimmel and Matthew W. Tufts
Hypersonic Sciences Branch
High Speed Systems Division

NOVEMBER 2017
Interim Report

DISTRIBUTION STATEMENT A: Approved for public release. Distribution is unlimited.

AIR FORCE RESEARCH LABORATORY
AEROSPACE SYSTEMS DIRECTORATE
WRIGHT-PATTERSON AIR FORCE BASE, OH 45433-7542
AIR FORCE MATERIEL COMMAND
UNITED STATES AIR FORCE

NOTICE AND SIGNATURE PAGE

Using Government drawings, specifications, or other data included in this document for any purpose other than Government procurement does not in any way obligate the U.S. Government. The fact that the Government formulated or supplied the drawings, specifications, or other data does not license the holder or any other person or corporation; or convey any rights or permission to manufacture, use, or sell any patented invention that may relate to them.

This report was cleared for public release by the USAF 88th Air Base Wing (88 ABW) Public Affairs Office (PAO) and is available to the general public, including foreign nationals.

Copies may be obtained from the Defense Technical Information Center (DTIC) (http://www.dtic.mil).

AFRL-RQ-WP-TP-2017-0169 has been reviewed and is approved for publication in accordance with assigned distribution statement.

REPORT DOCUMENTATION PAGE

Form Approved
OMB No. 0704-0188

The public reporting burden for this collection of information is estimated to average 1 hour per response, including the time for reviewing instructions, searching existing data sources, gathering and maintaining the data needed, and completing and reviewing the collection of information. Send comments regarding this burden estimate or any other aspect of this collection of information, including suggestions for reducing this burden, to Department of Defense, Washington Headquarters Services, Directorate for Information Operations and Reports (0704-0188), 1215 Jefferson Davis Highway, Suite 1204, Arlington, VA 22202-4302. Respondents should be aware that notwithstanding any other provision of law, no person shall be subject to any penalty for failing to comply with a collection of information if it does not display a currently valid OMB control number. **PLEASE DO NOT RETURN YOUR FORM TO THE ABOVE ADDRESS**.

1. REPORT DATE *(DD-MM-YY)*	2. REPORT TYPE	3. DATES COVERED *(From - To)*
November 2017	Interim	26 February 2015 – 01 July 2017

4. TITLE AND SUBTITLE
ANALYSIS OF WINDWARD SIDE HYPERSONIC BOUNDARY LAYER TRANSITION ON BLUNTED CONES AT ANGLE OF ATTACK

5a. CONTRACT NUMBER
In-house

5b. GRANT NUMBER

5c. PROGRAM ELEMENT NUMBER
61102F

6. AUTHOR(S)
Roger L. Kimmel and Matthew W. Tufts

5d. PROJECT NUMBER
3002

5e. TASK NUMBER

5f. WORK UNIT NUMBER
Q1FN

7. PERFORMING ORGANIZATION NAME(S) AND ADDRESS(ES)
Hypersonic Sciences Branch
High Speed Systems Division
Air Force Research Laboratory, Aerospace Systems Directorate
Wright-Patterson Air Force Base, OH 45433-7542
Air Force Materiel Command, United States Air Force

8. PERFORMING ORGANIZATION REPORT NUMBER
AFRL-RQ-WP-TP-2017-0169

9. SPONSORING/MONITORING AGENCY NAME(S) AND ADDRESS(ES)
Air Force Research Laboratory
Aerospace Systems Directorate
Wright-Patterson Air Force Base, OH 45433-7542
Air Force Materiel Command
United States Air Force

10. SPONSORING/MONITORING AGENCY ACRONYM(S)
AFRL/RQHF

11. SPONSORING/MONITORING AGENCY REPORT NUMBER(S)
AFRL-RQ-WP-TP-2017-0169

12. DISTRIBUTION/AVAILABILITY STATEMENT
DISTRIBUTION STATEMENT A: Approved for public release. Distribution is unlimited.

13. SUPPLEMENTARY NOTES
PA Clearance Number: 88ABW-2016-6030 Clearance Date: 23 Nov 2016

14. ABSTRACT
The seven-degree half-angle cone is a canonical geometry for high-speed boundary-layer transition. This paper presents constant N-Factor transition predictions for the Mack 2nd Mode along the windward plane for this geometry at differing angles of attack and differing nose radii in preparation for an upcoming experimental series. The stability analyses are able to capture the experimental trends seen in previous experiments. Computationally derived entropy swallowing lengths are shown to largely match the trends derived analytically in previous studies. These entropy swallowing lengths appear to be applicable as a figure of merit for transition studies, even at angles of attack. Bluntness appears to delay the amplification of Mack 2nd mode instabilities along the attachment line, rather than increasing the critical amplitude leading to transition. As is the case for cones at zero angle of attack, when transition occurs within the swallowing distance along the attachment line, it does not appear to be well-correlated with PSE/LST N-Factors.

15. SUBJECT TERMS
boundary layer transition, hypersonic, ground test

16. SECURITY CLASSIFICATION OF:			17. LIMITATION OF ABSTRACT:	18. NUMBER OF PAGES	19a. NAME OF RESPONSIBLE PERSON (Monitor)
a. REPORT	b. ABSTRACT	c. THIS PAGE			Roger L. Kimmel
Unclassified	Unclassified	Unclassified	SAR	19	19b. TELEPHONE NUMBER (Include Area Code) N/A

AIAA SciTech Forum
9 - 13 January 2017, Grapevine, Texas
55th AIAA Aerospace Sciences Meeting

American Institute of Aeronautics and Astronautics
Cleared for Public Release, Case Number: 88ABW-2016-6030

This material is declared a work of the U.S. Government and is not subject to copyright protection in the United States.

AIAA 2017-0764

Downloaded by AFRL D'Azzo Wright-Patterson on June 19, 2017 | http://arc.aiaa.org | DOI: 10.2514/6.2017-0764

Analysis of Windward Side Hypersonic Boundary Layer Transition on Blunted Cones at Angle of Attack

Matthew W. Tufts,* and Roger L. Kimmel†

Air Force Research Laboratory, Aerospace Systems Directorate, WPAFB, OH 45433-7542

The seven-degree half-angle cone is a canonical geometry for high-speed boundary-layer transition. This paper presents constant N-Factor transition predictions for the Mack 2nd Mode along the windward plane for this geometry at differing angles of attack and differing nose radii in preparation for an upcoming experimental series. The stability analyses are able to capture the experimental trends seen in previous experiments. Computationally derived entropy swallowing lengths are shown to largely match the trends derived analytically in previous studies. These entropy swallowing lengths appear to be applicable as a figure of merit for transition studies, even at angles of attack. Bluntness appears to delay the amplification of Mack 2nd mode instabilities along the attachment line, rather than increasing the critical amplitude leading to transition. As is the case for cones at zero angle of attack, when transition occurs within the swallowing distance along the attachment line, it does not appear to be well-correlated with PSE/LST N-Factors.

Nomenclature

Subscripts

c	condition at wall, inviscid (Taylor-Maccoll) solution
e	condition at boundary layer edge
w	condition at wall, viscous
∞	condition in freestream

Conventions

LST	Linear Stability Theory
PSE	Parabolized Stability Equations

Symbols

C_{sw}	swallowing length coefficient
$f(\eta_e)$	non-dimensional stream function (Levy-Lees/Lees-Dorodnitsyn transformed coordinates) calculated at B.L. edge at point where entropy layer is swallowed
h_0	total enthalpy
M_s	Mach number at spherical shoulder, inviscid solution
R	specific gas constant
R_n	cone nose radius
Re'	freestream unit Reynolds number, $\frac{u_\infty}{\nu_\infty}$
X_{sw}	entropy swallowing length
X_{TB}	blunt cone transition location
X_{TS}	sharp cone transition location
$\overline{y}$	non-dimensional distance to conical shock
α	angle of attack
γ	specific heat ratio

*Research Engineer, Ohio Aerospace Institute, Member AIAA
†Senior Research Engineer, Associate Fellow AIAA

DISTRIBUTION STATEMENT A: Approved for public release;
Distribution is unlimited.

λ	characteristic coefficient of viscosity, $\frac{\mu}{T^{1/2}}$
θ_{cone}	cone half-angle
θ_{inc}	windward included angle

I. Introduction

A Key factor in the design of a hypersonic vehicle is a reasonable method of predicting the boundary layer transition to turbulence. A PSE-based e^N method using a constant N-factor has performed remarkably well in correlating wind tunnel transition on cones with small bluntness at zero angle of attack.[1] However, the addition of even a small amount of geometrical complexity in the form of AoA creates rather complex changes in the transition behavior on cones. As a point of reference, consider the windward meridian of a cone at AoA. This is also a practical consideration, due to the increased heating on the cone attachment line.

Although, as noted by Stetson,[2] the behavior of windward-side transition on cones at AoA in hypersonic flow can vary widely among different data sets, some general trends are consistent. For sharp cones, as AoA increases, windward transition moves downstream.[2–4] Blunt cones showed a more complex trend. Stetson[2] observed windward transition on blunt cones to move downstream for small AoA, up to some maximum displacement. The angle of attack producing the maximum downstream displacement varied with nose bluntness. At higher AoAs, transition moved upstream as AoA increased.

Some variations in the behavior of blunt cone windward transition at AoA have been observed. Stetson and Rushton[3] saw only monotonic upstream movement of windward transition for two bluntnesses on an 8° cone at M = 5.5. Holden[5] saw downstream movement of the windward transition front on a sharp and 6% blunt cones, but upstream movement for a 21% blunt cone at M = 11 and 13. Tests of the HIFiRE-1 blunt cone at CUBRC[6–8] at M = 6.6 and 7.2 showed little movement of the windward transition front for 1° AoA, and upstream movement at 2° and 5° AoA. Tests of HIFiRE-1 at NASA LaRC[9] showed slight downstream movement of the windward transition front at AoA = 3° and 5°. Juliano et al.[10] showed no movement of the windward transition front (within transducer resolution) with increasing angle of attack for AoA $\leq 6°$, and downstream movement for higher AoAs.

Although a constant N-factor of N = 5.5 worked well to correlate transition for HIFiRE-1 at zero AoA, it was less successful for correlating windward transition at AoA.[1] N-factor calculations using PSE on the windward centerline of HIFiRE-1 for NASA LaRC test conditions showed N-factors exceeding 8 for AoA of both 3° and 5°. However, the windward boundary layers remained laminar in the wind tunnel at both AoAs. This behavior was difficult to reconcile with the good correlation obtained for AoA = 0°.

For zero AoA conditions Lei and Zhong[11] showed that increases in nose bluntness consistently delayed the onset of second mode instabilities.

For non-zero AoA cases, Alba[1] applied an axisymmetric PSE analysis to the windward centerline flowfield derived from a 3D basic state calculation, since tools accounting for three-dimensionality were unavailable to him at the time, and this was noted as a source of uncertainty. Several other possible complicating factors might explain the difficulty in adapting a constant N-factor prediction method to the windward side of cones at AoA. A partial list of complications includes changes in edge Mach number, edge unit Reynolds number, dominant instability frequency, dependence of initial amplitude upon frequency, and entropy swallowing lengths.

Given the very complex behavior of cone attachment line transition at AoA, and the limited success in correlating it, a systematic investigation is suggested, starting with non-axisymmetric PSE analysis and attempting to reduce uncertainties cited by Alba et al. moving towards implementing three-dimensional formulations and analyzing flow away from the windward meridian. Recently, in preparation for a series of tests on cones at AoA, Jewell and Kimmel[12] performed zero-degree AoA, axisymmetric computations using stability theory to predict the transition on cones with differing nose radii at Stetson's[2] conditions. Jewell and Kimmel showed that the calculated 2nd mode N-Factor at the observed experimental transition location decreases rapidly when transition is within the entropy swallowing distance. The current paper continues this effort by extending the LST/PSE analysis to the windward meridian of cones at AoA. In addition, the mean flow field on the attachment line is carefully examined in an attempt to provide heuristic explanations of the windward stability behavior.

Downloaded by AFRL D'Azzo Wright-Patterson on June 19, 2017 | http://arc.aiaa.org | DOI: 10.2514/6.2017-0764

DISTRIBUTION STATEMENT A: Approved for public release;
Distribution is unlimited.

Downloaded by AFRL D'Azzo Wright-Patterson on June 19, 2017 | http://arc.aiaa.org | DOI: 10.2514/6.2017-0764

II. Reference Experiment

II.A. Model Geometry

A a 7° half-angle, spherically blunted, circular cone with a base radius of 2 inches (50.8 mm) and interchangeable nose-tip pieces to allow for changing of the nose radius has been fabricated for a planned experiment in the AFRL High Reynolds Number Facility and AFRL Ludweig Tube. The available values of nose radius and bluntness ratio are tabulated in Table 1. For a perfectly sharp cone, the geometry would result in a cone length of 16.3 inches (413.7 mm).

Given the relatively short planned run times, the wall temperature has been assumed to be roughly ambient ($T_w = 300K$) and isothermal as the model is not expected to experience significant heating during course of a run. For the conditions planned, this gives a $T_w/T_{aw} = 0.57$ and $T_w/T_0 = 0.49$.

Note that this cone, in order to better compare with recent experiments is planned for a 7° half-angle cone, as opposed to the 8° half-angle used in the original Stetson[2] experimental series. At the time of writing, the experiment is planned for late November 2016.

Bluntness	Nose Radius		Total Length	
%	(mm)	(in)	(mm)	(in)
"sharp" (0.35)	0.18	0.007	413.7	16.3
1.0	0.508	0.02	410.1	16.1
3.0	1.524	0.06	402.8	15.9
5.0	2.54	0.10	395.4	15.6
10.0	5.08	0.20	377.1	14.8
20.0	10.16	0.40	340.5	13.4
30.0	15.24	0.60	303.9	12.0

Table 1. Cone Geometry Parameters

II.B. Freestream Conditions

Flow conditions used for the study model those found in the AFRL High Reynolds Number Facility. The facility is a blowdown tunnel equipped with a constant-geometry, axisymmetric nozzle having an exit diameter of 12.3 inches, resulting in a test core with an approximately 10 inch diameter. The nozzle is operated with nominal stagnation pressures ranging from 700 to 2100 pisa (4.8 MPa - 14.5 MPa), and a nominal stagnation temperature of 1100° R (611 K). These conditions result in unit Reynolds numbers that range from roughly 30×10^6/m to 90×10^6/m. Full conditions that result from this operating range are listed in Table 2.

P_0	Unit Reynolds Number		ρ_∞	P_∞	T_∞	U_∞	M_∞
(psia)	($\times 10^6$/m)	($\times 10^6$/in)	(kg/m^3)	(Pa)	(K)	(m/s)	
700	30.4	0.77	0.154	3388.8	76.75	1036.19	5.90
1400	60.9	1.54	0.308	6777.5	76.75	1036.19	5.90
2100	91.3	2.32	0.461	10166.3	76.75	1036.19	5.90

Table 2. Nominal Flow Parameters - AFRL High Reynolds Number Facility

Available details on the flow parameters in the wind tunnel can be found in Fiore and Law.[13] The nozzle can be assumed to produce conventional (non-quiet) acoustic noise levels, justifying the choice of a relatively low second mode transition N-factor (N = 4) for analysis.

III. Methods

III.A. Computational Grid

Multi-block topology grids used for the study were created using Pointwise glyph scripts. Computationally, the model was assumed to be smooth (no modeled surface roughness) with a perfectly spherical tip. The nose was represented by projecting a square mesh onto the spherical nose tip, similar to the cartoon of

DISTRIBUTION STATEMENT A: Approved for public release;
Distribution is unlimited.

Figure 1, and subsequently smoothing the projected shape to blend smoothly with a conical grid placed on the frustum. A symmetry plane was included to reduce computational expense. Wall-normal spacing in terms of y+ was less than 1 everywhere on the surface, except very near the stagnation point, where the boundary layer is extremely thin.

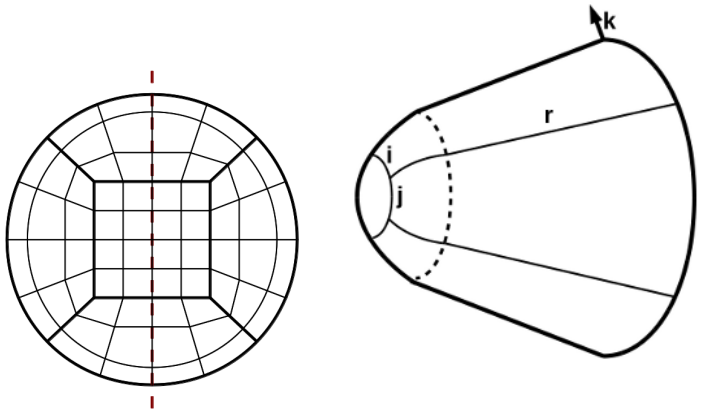

(a) Grid Topologies (b) Grid Coordinates

Figure 1. Cartoon of Grid Topology

Due to the changing nose radii, and changing overall cone length, the total number of grid points in each grid, but the average is approximately 50 million points. The grid topology can be found in Table 3.

Configuration	"i" Pnts.	"j" Pnts.	"k" Pnts.	"r" Pnts.
Sharp (0.35% Blunt)	51	67	353	869
1% Blunt	59	77	353	857
3% Blunt	59	77	353	839
5% Blunt	59	77	353	821
5% Blunt (Medium)	47	63	283	643
5% Blunt (Coarse)	39	51	227	515
10% Blunt	59	77	353	773
20% Blunt	59	77	353	673
30% Blunt	87	115	353	643

Table 3. Grid Resolution Figures

III.B. Computational Methods

The US3D[14] flow solver[a] with 2nd-Order Steger-Warming fluxes was used to solve for the basic states. In keeping with laminar-flow stability studies, no turbulence models were needed, as the base-state flow is necessarily considered to be laminar everywhere. In general, a balance between taking a time step large enough to facilitate reasonable convergence while maintaining numerical stability was striven for. A maximum timestep on the order of $1.0e^{-8}$ seconds was used, accordingly in the smallest cells near the nose the maximum CFL is on the order of 100.

The LASTRAC[15,16] stability suite was used to solve the LST/PSE stability equations. An in-house Fortran script converted the US3D unstructured cell-centered solution to LASTRAC3d[17] formatted meanflow file without interpolation.

Because the meanflow in the vicinity of the windward ray has relatively few rapid changes in the azimuthal direction, assuming azimuthal homogeneity (i.e. PSE and LST) can be used to compute 2nd mode growth rates. As seen in Figure 2, because there is zero curvature in the axial direction and small non-parallel effects due to the high Reynolds numbers, PSE and LST show reasonable agreement for these cases.

[a] US3D 1.0-RC22

Downloaded by AFRL D'Azzo Wright-Patterson on June 19, 2017 | http://arc.aiaa.org | DOI: 10.2514/6.2017-0764

DISTRIBUTION STATEMENT A: Approved for public release;
Distribution is unlimited.

It was also found that inclusion of corrections for spanwise non-uniformity as implemented in the LASTRAC3d formulation resulted in minimal changes in stability behavior, even along the shoulder of the cone where spanwise non-uniformity is stronger than along the windward plane.

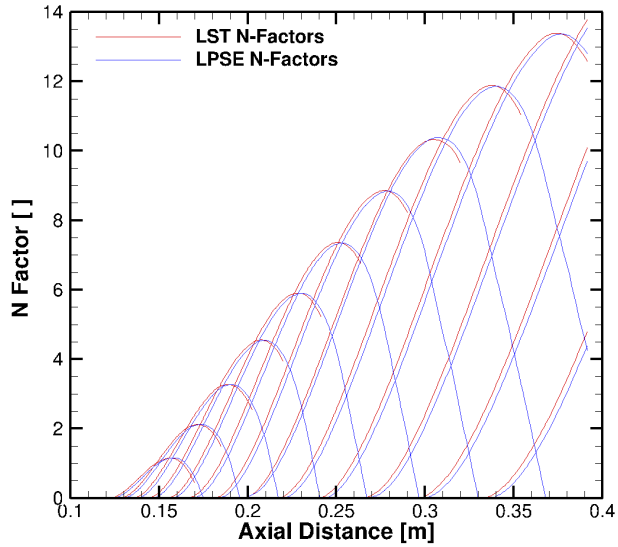

Figure 2. Comparison of PSE and LST N-Factors, 5% Bluntness, 5° AoA, Re' = 30 M/m

IV. Flow Features

IV.A. Crossflow Instabilities

As has been noted in literature[18,19] the crossflow instability can be seeded even due to grid-to-grid roughness. This leads to distortion of the base state, and if the instability reaches an amplitude great enough to affect the stability analyses, may preclude meaningful results in the areas that are affected.

The question arises as to whether or not this is a physical mechanism, or some feature due to the numerics. If one computes the stationary N-Factors for the configuration using meanflows containing these vortices, assuming that the distortion arising from the vortices does not totally divorce the computed results from reality, as seen in Figure 3 the maximum N-Factor reaches above 30. This corresponds to an amplification ratio above 1×10^{13}. It is therefore not surprising that stationary crossflow vortices are present in the Navier-Stokes calculations.

Downloaded by AFRL D'Azzo Wright-Patterson on June 19, 2017 | http://arc.aiaa.org | DOI: 10.2514/6.2017-0764

DISTRIBUTION STATEMENT A: Approved for public release;
Distribution is unlimited.

Downloaded by AFRL D'Azzo Wright-Patterson on June 19, 2017 | http://arc.aiaa.org | DOI: 10.2514/6.2017-0764

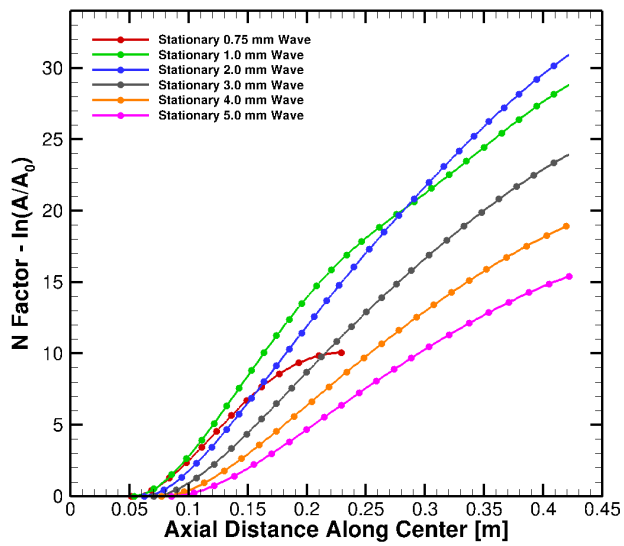

Figure 3. Sample Crossflow N-Factors Along 90° Ray, 5% Bluntness, 5° AoA, Re' = 60 M/m

This effect can be lessened by careful smoothing of the surface grid, or alternatively by coarsening of the mesh (and thus increasing the dissipation) as suggested by Dinzl and Candler.[19] For this study, it was found the appearance of these crossflow vortices could be reduced to a level that did not impact the windward meridian second mode analysis, as discussed in the next section. However, somewhat counter-intuitively but confirmed in literature, increased grid resolution causes the appearance of these undesired flow distortions to become higher in wavenumber and higher in amplitude.

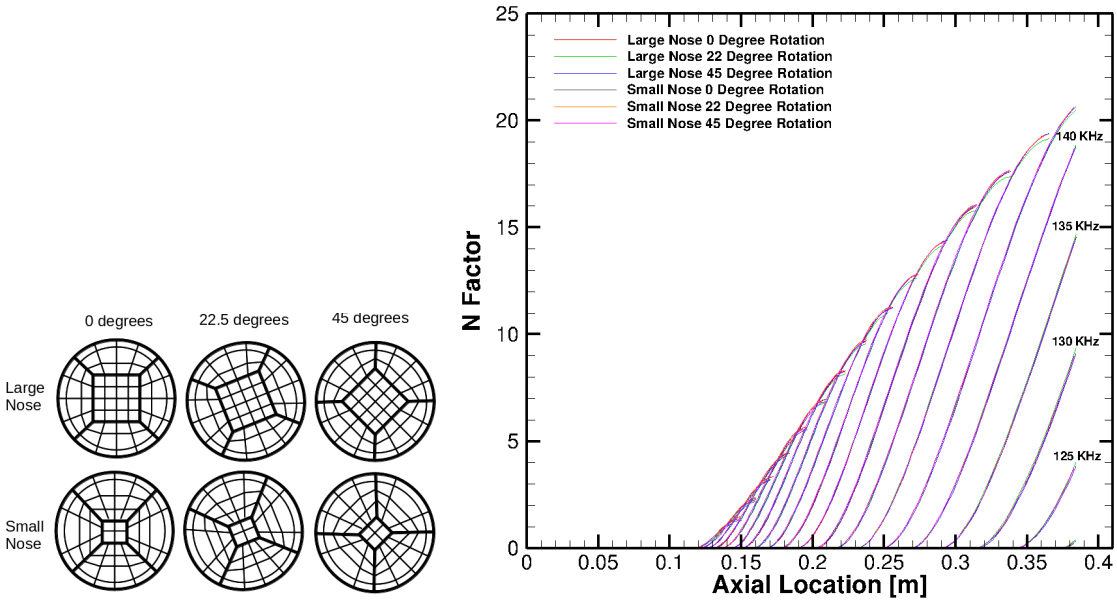

(a) Grid Topologies

(b) 2nd Mode Windward N Factors

Figure 4. Windward Stability Comparison 5% Bluntness, 5° AoA, Re' = 60 M/m

IV.B. Grid Topology Study

Grid convergence was judged by calculating the desired solution functional, the windward 2nd mode stability characteristics. To test the effects of the nose-seeded instability waves six different nose configurations were calculated seen in Figure 4(a). For this portion of the study, the grid configurations were tested using a bluntness ratio of 5%, Re' = 60 M/m, and AoA = 5°. The second mode stability behavior converges well,

DISTRIBUTION STATEMENT A: Approved for public release;
Distribution is unlimited.

as in Figure 4(b).

IV.C. Grid Resolution Study

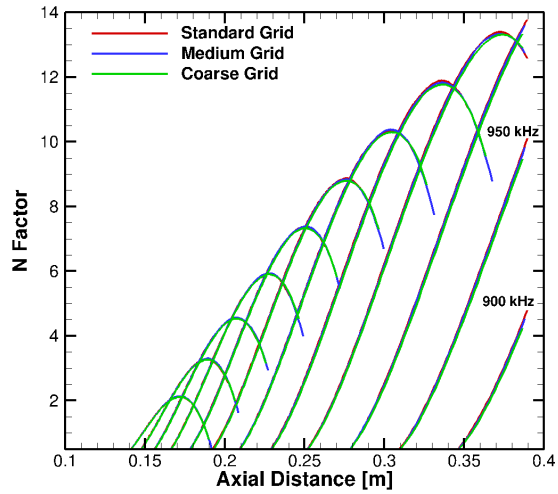

Figure 5. 2nd Mode Windward N-Factors 5% Bluntness, 5° AoA, Re' = 30 M/m

Given the number of cases examined, full grid convergence studies were not done for each configuration. However, a sample case (5% Bluntness, 5°, Re' = 30M/m) can be seen in Figure 5. The changes in the N-Factor for a given frequency were found to be acceptable.

IV.D. Overexpansion

As has been experienced in previous studies[20,21] certain combination of flow conditions may result in an overexpansion of the flow moving around the shoulder of the nose tip onto the frustum. In cases where this situation occurs on conical geometries, the resulting expansion and compression waves reflect from both the shock surface and from slip lines in the flow, causing an inflection in the shape of the shock. As the angle of attack increases, this effect becomes more and more prominent.

V. Entropy Swallowing

The entropy swallowing location for a blunted cone is physically defined according to Stetson[22] as the location where the fluid at the edge of the boundary layer has passed through a nearly conical shock, and hence the edge conditions are close to those that would be experienced on a perfectly sharp cone. As Stetson noted, the entropy swallowing length is somewhat ill-defined. However, when a consistent method is applied, entropy swallowing is a useful metric to describe the extent of the entropy layer effects on a body. Stetson and others[2,3,22–24] developed methods to estimate entropy swallowing distances at 0 AoA. In order to understand the behavior of cones at non-zero AoA it is useful to develop an estimation of entropy swallowing distance on yawed cones.

Zakkay and Krause[23] used analytical solutions for conical flows to find the following closed expression for entropy swallowing distance based on comparing the mass flow rate through the bow shock to the mass flow rate through the boundary layer on an axisymmetric cone at zero AoA.

$$\frac{X_{sw}}{R_n} = \left[\frac{3}{2}\frac{(R/\gamma)^{1/2}}{\lambda\, p_c}\;\frac{{\rho_\infty}^2{U_\infty}^2}{3M_c + M_s}\;\frac{\overline{y}^4 R_n}{f^2(\eta)\sin^2\theta_{cone}}\right]^{1/3} \tag{1}$$

Following Rotta[24] equation (1) can be rearranged to the form

$$X_{sw} = C_{sw}\; {Re'}^{(1/3)}\; {R_n}^{(4/3)} \tag{2}$$

DISTRIBUTION STATEMENT A: Approved for public release;
Distribution is unlimited.

Downloaded by AFRL D'Azzo Wright-Patterson on June 19, 2017 | http://arc.aiaa.org | DOI: 10.2514/6.2017-0764

where

$$C_{sw} = \left[\frac{3}{2}\frac{p_\infty}{p_c}\frac{M_\infty}{3M_c + M_s}\frac{\overline{y}^4}{f^2(\eta)\sin^2\theta_{cone}}\right]^{1/3} \tag{3}$$

where $C_{sw} = C_{sw}(\theta_{cone}\,,\, M_\infty)$ is a constant based only on cone angle and freestream Mach number. Note that Re', R_n, and X_{sw} must use consistent units. Stetson[22] provides a convenient graphical representation of the coefficient for a range of cone angles, and a range of freestream Mach numbers. However, as is noted in Stetson,[22] because $\overline{y}$ used appears as a quartic term in the analytical expression: "*The swallowing distance is a somewhat ambiguous length, since it depends upon the chosen shock shape and definition of the boundary of the entropy layer, and the choice of boundary layer assumptions. Therefore one should not think of the swallowing length as a precise dimension.*"

Implicit in the development of these equations is the assumption of an axisymmetric flowfield. Commonly used geometric fits for shock shape e.g. Klaimon,[25] Billig[26] are also limited to axisymmetric configurations. However, an approximation for the windward plane can be found by using the above solution, Equation (1) but replacing the cone half angle (θ_{cone}) with the included angle along the windward plane (θ_{inc}) where

$$\theta_{inc} = \theta_{cone} + \alpha \tag{4}$$

Note that this substitution was made in all steps of the calculation (e.g. θ_{inc} was used to calculate the Taylor-Maccoll parameters, shock angle, etc.)

V.A. Swallowing Distance Trend with AoA

Examining Equation (2) it is apparent that the swallowing distance scales by nose radius with a 4/3 power law, and with Reynolds number by a 1/3 power law. However, less obvious by inspection, the changing terms in Equation (3) result in a decrease of C_{sw} with increasing θ_{cone} for fixed freestream conditions (e.g. Figure 5 in Stetson[22]). If the usage of θ_{inc} holds for cones at angle of attack, accordingly the swallowing distance along the windward plane decreases for a given cone with increasing α.

V.B. Computational Swallowing Distance

Rather than using analytical solutions, one can use a computational method to calculate entropy swallowing distances. Two approaches were taken to find the entropy swallowing lengths for cones at AoA. The first method is based on the same definitions used by Zakkay and Krause to derive their expression. In the second method, a swallowing criterion is defined and calculated directly.

Finding boundary layer thicknesses in hypersonic flows is often ambiguous in nature since there is often not an obvious choice for edge conditions. We may define our boundary layer thickness δ_h defined as the point farthest away from the wall where

$$\left|1 - \frac{h_0(y) - (h_0)_w}{(h_0)_\infty - (h_0)_w}\right| > 0.1\% \tag{5}$$

Doing so gives a convenient and consistent measure of boundary layer thickness.

In order to directly follow Zakkay and Krause, one can use a Taylor-Maccoll solution to determine the Mach number downstream of the sharp conical shock and at the surface. Then finding the point on the computed shock where the flow behind the shock results in a Mach number 95% of the surface Mach number when expanded to surface pressure, denotes the start of the "conical shock". One can then draw an annulus between this point and the cone surface, and integrate between the two points to find the mass flow rate through this annulus (bow shock annulus). This mass flow rate represents the mass ingested through the bow shock. Using Equation (5) to find the BL edge, one can also integrate from the cone surface to the bl edge. At the farthest upstream location where the mass flow through the boundary layer is equal to or greater than the mass flow through the bow shock annulus, the entropy layer is considered swallowed.

When applying this algorithm to axisymmetric flow, as done analytically, the choice of azimuthal angle is inconsequential. Due to the change in flow azimuthally for cones at angle of attack, the choice was made for the current study to find the conical shock location on the windward plane. The resulting annulus was drawn in a plane normal to the cone's axis from the cone surface to the shock at this axial location, despite

Downloaded by AFRL D'Azzo Wright-Patterson on June 19, 2017 | http://arc.aiaa.org | DOI: 10.2514/6.2017-0764

DISTRIBUTION STATEMENT A: Approved for public release;
Distribution is unlimited.

the difference in conditions as azimuthal angle changes. For the cases studied, this method for the most part closely reproduced the curves given by evaluating the analytical expression, however cases at higher AoA showed some inconsistent trends. This method also proved to be very sensitive to the definition of boundary layer thickness, as the mass flux near the edge of the boundary layer is high. In addition as one moves either farther downstream or farther from the wall, the area included in the annulus increases more rapidly due to the larger local radius of the annulus.

A more robust and somewhat simpler method is after finding the point on the computed shock where the expanded flow behind the shock results in a Mach number 95% of the surface Mach number, find the relative (to the freestream) entropy at this point. One can then march down the cone using Equation (5) to find the boundary layer edge. At the point where the entropy at this boundary layer edge is $\leq$ than 95% of the entropy found in the first step, the entropy layer is considered swallowed. A comparison of the analytical method and this computational method can be seen in Figure 6. It can be seen that the trends found by the analytical method and the computational methods largely agree, however the constants (C_{SW}) differ by a factor of 2. This is not unexpected, given that the swallowing distance is not easily defined, and is used only as a figure of merit for extracting trends. Note however, that by examining Figure 6 it appears that at 5° AoA, the windward swallowing distance scales somewhat more weakly with R_N than at 0° AoA.

This method also has the advantage of removing the ambiguity in choosing the angle of the slice chosen to be the annulus, as well allowing for the acknowledgment that entropy swallowing length varies with meridian of the cone when the flow is non-axisymmetric. This variation can be seen in Figure 6(b).

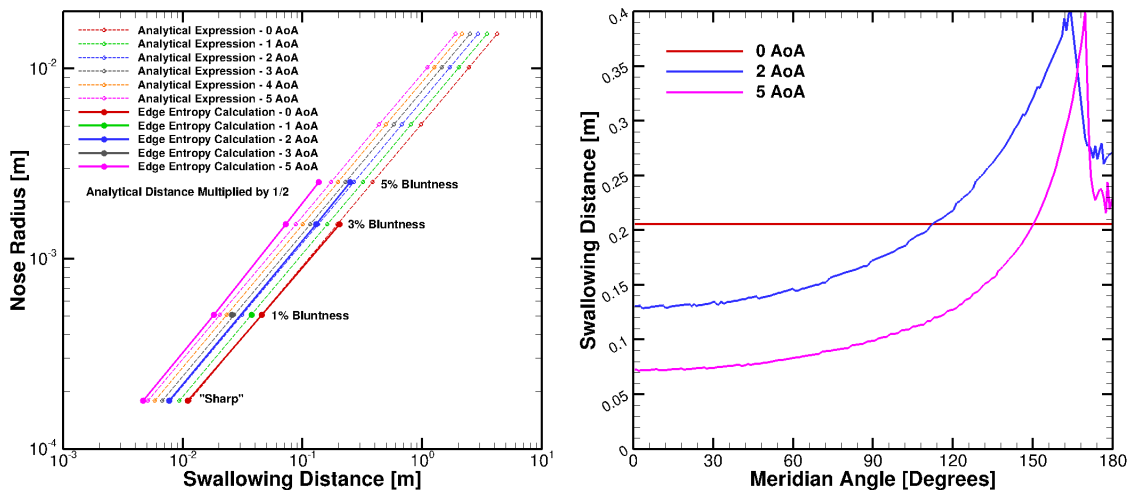

(a) Compared with Analytical (Windward Plane)

(b) Plotted vs. Meridian Angle, 3% Bluntness

Figure 6. CFD Calculated Swallowing Distance

VI. Stability Results

Once base states have been calculated, these can be used to calculate stability behavior. For this study, only second mode instabilities along the windward ray are considered.

It was observed by Juliano et al.[27] in an examination of HIFiRE-1 wind tunnel data that the effect of increasing nose bluntness was to decrease the pressure fluctuations observed at a given Reynolds number and a given station along a cone. Furthermore, Juliano et al. noted that the maximum pressure fluctuation amplitudes observed were similar for different bluntnesses. These results suggest that the effect of increasing nose bluntness is to delay amplification of second mode instabilities, rather than to increase the critical amplitude required for breakdown. The "e^N method", as commonly applied, is based upon the premise that once a disturbance has reached some critical amplitude, transition to turbulence follows. Because stability theory predicts only the amplification of disturbances, a critical aspect of the e^N method is selecting a correlating transition N-Factor. Note the choice of transition N-Factor is essentially equivalent to modeling the receptivity process to the freestream disturbance spectra. Good comparisons between computation and experiment were obtained for HIFiRE-1 wind tunnel data using a constant N-Factor of 4 for noisy wind tunnels. Recent work at higher Mach and Reynolds numbers[12,28,29] have indicated that a higher N-factor

Downloaded by AFRL D'Azzo Wright-Patterson on June 19, 2017 | http://arc.aiaa.org | DOI: 10.2514/6.2017-0764

DISTRIBUTION STATEMENT A: Approved for public release;
Distribution is unlimited.

may provide better correlations under these conditions and that the correlating N-Factor may depend on the particular frequency that provokes transition, due to differences in the initial disturbance spectrum. However, at this time variable N-Factor methods are not yet mature.

Second mode instabilities, are therefore assumed to be equally forced at all frequencies in a conventional hypersonic wind tunnel (equal initial disturbance amplitudes). At the farthest upstream location which the second mode envelope reaches the selected N-Factor, the resulting point is denoted as the estimated transition location. Tests of HIFiRE-1 at zero AoA indicated a correlating N-Factor of about 4 for noisy wind tunnels. Jewell and Kimmel[12] showed correlating N-Factors of about 7-8 for sharp and slightly blunted cones at zero AoA in the AFRL High Reynolds Number Facility where Stetson's experiments were carried out. Therefore, N-Factors of 4 and 7 were chose for the current analysis. The results of this algorithm can be seen in Figure 7. The quantitative characteristics change with the choice of transition N-Factor, as would be expected. However, with the notable exception that the transition location crossover starts at a lower AoA with higher transition N-Factors, there is little qualitative change due to this choice in both the trends shown and the hypothesized explanations for the observed trends.

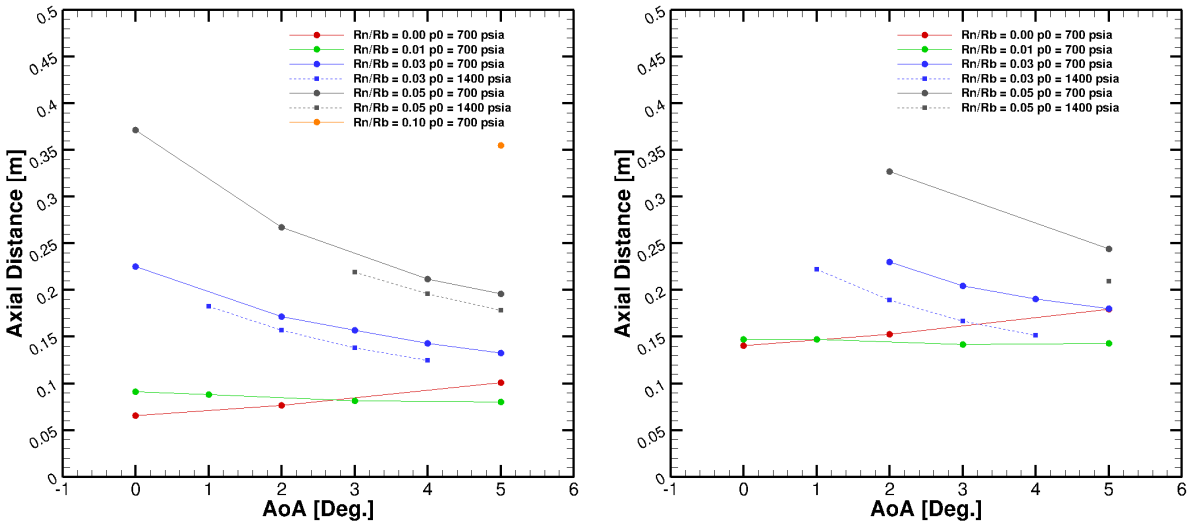

(a) N=4 (b) N = 7

Figure 7. Computed 2nd Mode Transition Location (LST) Windward Plane

In general the results of this study are qualitatively similar to the experimental results available from Stetson[2] in that one would expect the windward transition to generally move downstream with angle of attack for sharp cases, and upstream for blunt cases. As can be seen in Figure 7, the case a 1% bluntness (a configuration not examined by Stetson) falls somewhere in-between and shows little movement along the windward plane with AoA changes. A discrepancy with the experimental results of Stetson is the magnitude of the transition front movement. If a constant N-Factor is used to predict transition location, the computational results predict larger amounts of movement than the experimental tests actually reported. In particular, for larger nose radii at low angle of attack the transition front is predicted downstream of the experimental results.

VI.A. Effects of Entropy Swallowing on Transition

An obvious trend is that the discrepancy between experimental and computational results increases as the analytical prediction of swallowing distance increases. Additionally, comparison of the experimental results of Stetson with computational results by Jewell and Kimmel[12] suggests that the transition 2nd mode N-Factor is approximately constant only when experimental transition occurs outside of the entropy swallowing region. Calculating the swallowing length using the methods employed by Zakkay and Krause, the current conditions for larger bluntnesses (above 1%) predict transition inside the swallowing region, therefore this difference is not unexpected.

If one plots the CFD calculated entropy swallowing length along with the N-factors, as seen in Figures 8 and 9 it becomes apparent that the first neutral point for second mode instabilities as calculated using

Downloaded by AFRL D'Azzo Wright-Patterson on June 19, 2017 | http://arc.aiaa.org | DOI: 10.2514/6.2017-0764

DISTRIBUTION STATEMENT A: Approved for public release;
Distribution is unlimited.

stability theory, at both axi-symmetric and at-angle of attack cases, appears to always be near this point for the cases examined. However, plotting the 1st neutral point location versus nose radius shows that the trend is closer to linear with nose radius rather than the 4/3 power law that would be suggested if the location of the 1st neutral point scaled directly with swallowing distance.

By following the envelope (maximum N-Factor at a given axial location) either on the raw plots like the one in Figure 8 or in the re-plotting given in Figure 10 it can be seen that while increasing bluntness moves the first neutral point rearward on the cone, the growth rates immediately after this point are also higher with increasing bluntness. This is supported by findings presented in both Stetson.[22] and in Juliano et al.[27] stating that the dominant effect is likely delaying the amplification of second mode instabilities rather than increasing the critical amplitude. It is interesting to note that while the entropy layer thickness near the nose will increase with nose bluntness, the boundary layer thickness as defined in equation 5 stays largely the same. This means that, downstream of the swallowing distance, given disturbances amplify similarly, regardless of nose bluntness. For example the 1000 kHz modes shown in in Figure 9 are quite similar, despite the change in entropy swallowing.

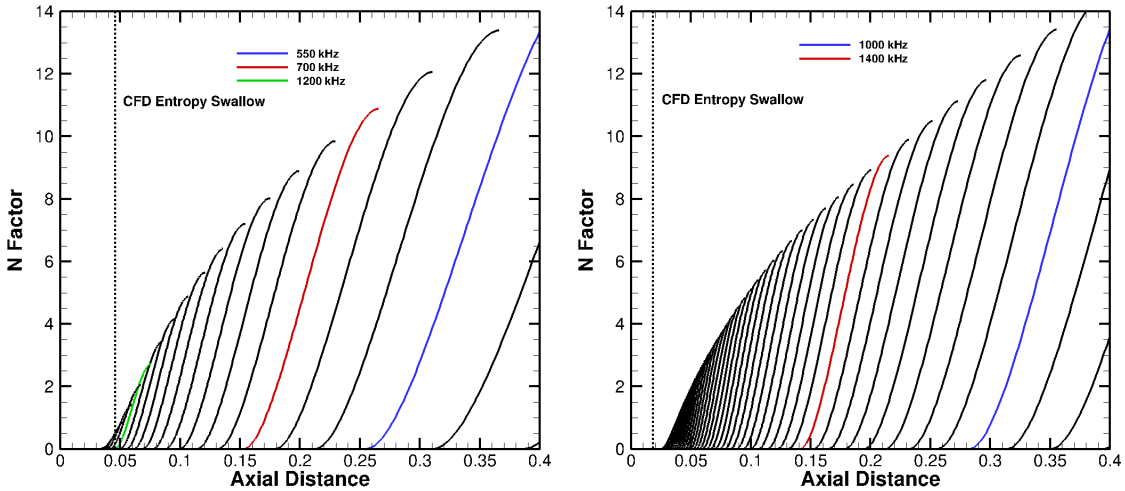

(a) 0° AoA (b) 5° AoA

Figure 8. Windward 2nd Mode N-Factors, 1% Bluntness, Re' = 30 M/m

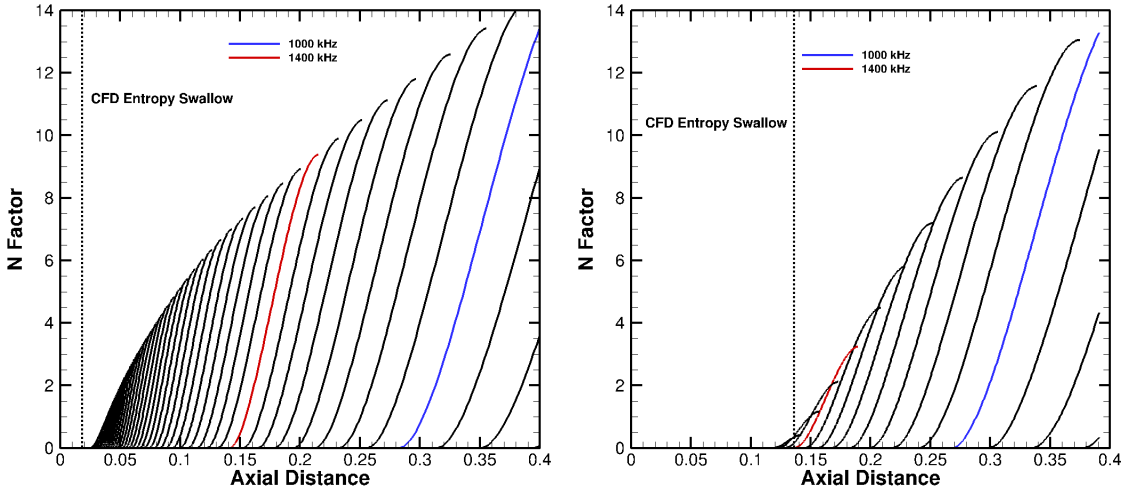

(a) 1% Bluntness (b) 5% Bluntness

Figure 9. Windward 2nd Mode N-Factors, 5° AoA, Re' = 30 M/m

Downloaded by AFRL D'Azzo Wright-Patterson on June 19, 2017 | http://arc.aiaa.org | DOI: 10.2514/6.2017-0764

DISTRIBUTION STATEMENT A: Approved for public release;
Distribution is unlimited.

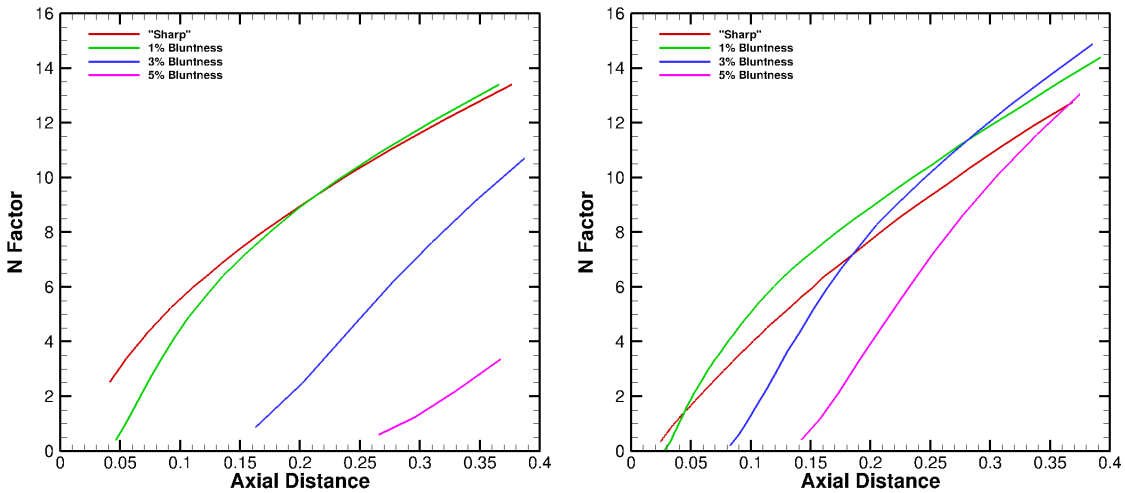

(a) 0° AoA (b) 5° AoA

Figure 10. Windward 2nd Mode N-Factor Envelopes, Re' = 30 M/m

Some of these effects can be explained heuristically by examining contours of local Reynolds number, as in Figure 11. It is difficult to compare across angles of attack (e.g. 5% bluntness 0° AoA to 5% bluntness 5° AoA) since many of the flow properties along the windward plane are changing. However, by comparing across bluntnesses at the same angle of attack, one can see that at zero angle of attack the effects of nose-bluntness affects the local Reynolds number. There is a fairly mild overexpansion, and therefore the accompanying recovery is also mild. The overall effect is therefore largely a reduction in the local Reynolds number for much of the cone, and a recovery to flow similar to the sharp conditions.

However, for a cone at angle of attack the overexpansion in pressure along the windward plane, and the accompanying recovery downstream, becomes stronger. The resulting recovery increases the local Reynolds number to above that of the sharp cone, leading to overall stronger growth once the region of high Reynolds number is reached. This area starts at approximately the CFD entropy swallowing distance, which provides some insight into the changes in N-Factor envelopes. However it should be noted again as before that this measure is problematic because the overexpansion features due to the shock appear to scale linearly with nose radius in the cases examined, instead of the 4/3 power law with nose radius as would be implied by a linear scaling with swallowing distance.

Downloaded by AFRL D'Azzo Wright-Patterson on June 19, 2017 | http://arc.aiaa.org | DOI: 10.2514/6.2017-0764

DISTRIBUTION STATEMENT A: Approved for public release;
Distribution is unlimited.

Downloaded by AFRL D'Azzo Wright-Patterson on June 19, 2017 | http://arc.aiaa.org | DOI: 10.2514/6.2017-0764

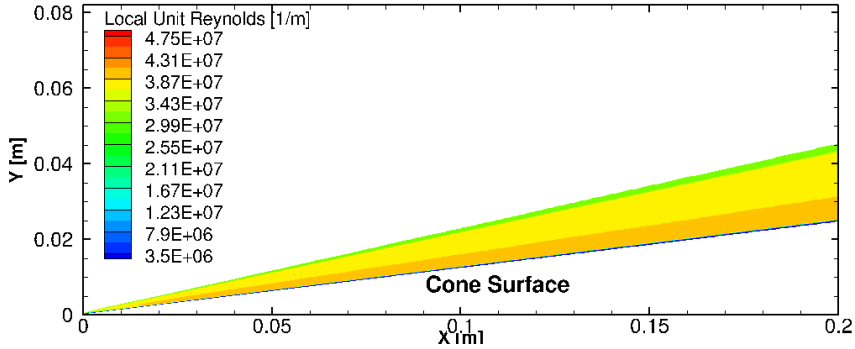

(a) Sharp - 0 AoA

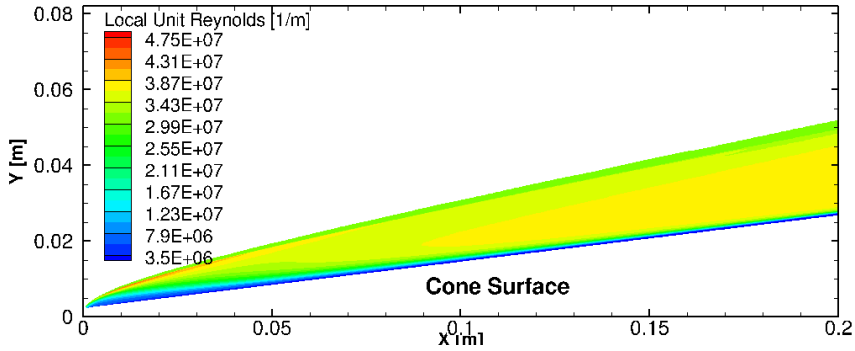

(b) 5% Bluntness - 0 AoA

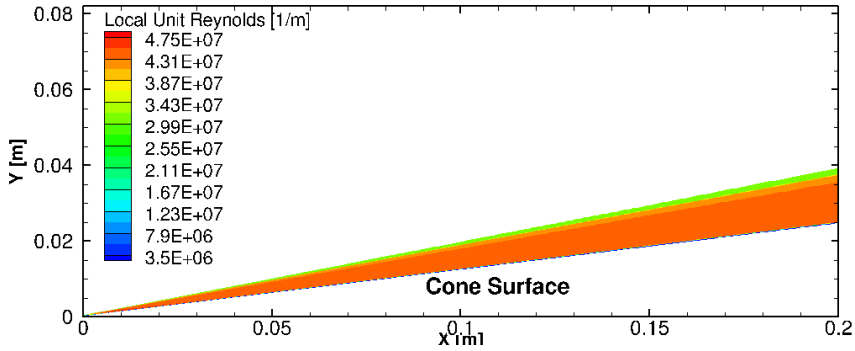

(c) Sharp - 5 AoA

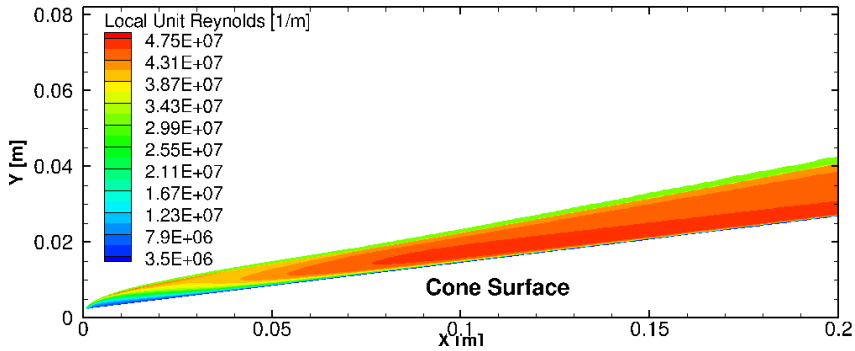

(d) 5% Bluntness - 5 AoA

Figure 11. Contours of Unit Reynolds Number (Windward Plane)

DISTRIBUTION STATEMENT A: Approved for public release;
Distribution is unlimited.

By non-dimensionalizing the data using the method of Stetson, one can make a direct comparison of the current computations to Stetson's experimental data. Figure 12 non-dimensionalizes transition distance by the swallowing distance, and angle of attack by cone half angle. Overall, the trends with angle of attack seen by Stetson are captured using a constant N-Factor method, with the exception of the movement downstream when going from small angles of attack to zero angle of attack for larger bluntnesses. For N = 7 the non-dimensionalized transition movement does not match the magnitude, although note that the slope of the lines appear to be approximately correct, and that Stetson's data are taken for two different unit Reynolds number. Because the attachment line boundary layer thins significantly with increasing AoA, the range of unstable second mode frequencies also increases with AoA. This shift in disturbance frequencies implies that a differences in initial disturbance amplitudes between frequencies would be reflected in the transition location. Because of this a variable N-Factor method (better modeling of receptivity) might better recover changes in the absolute movement of the transition front. N = 4 was also plotted, as this allowed data for more configurations to be shown as N = 4 was reached more easily. As seen in Figure 13, many of the predicted N=4 transition locations are well within the swallowing distance. Jewell and Kimmel's[12] analysis of Stetson's zero AoA data showed that a that the constant N-factor method was not applicable in this region, where calculated N-factors at transition were often < 2.

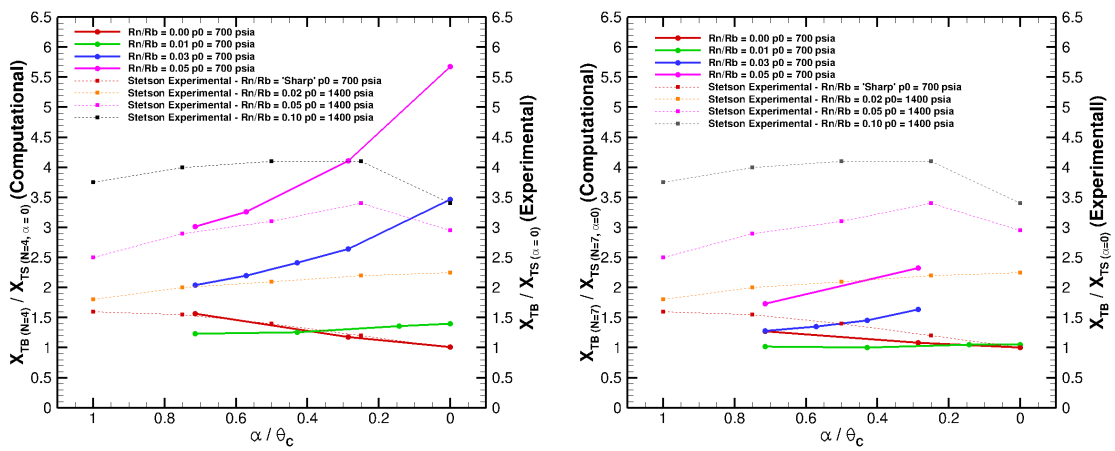

(a) N=4 (b) N=7

Figure 12. Non-Dimensional Transition (Style of Stetson)

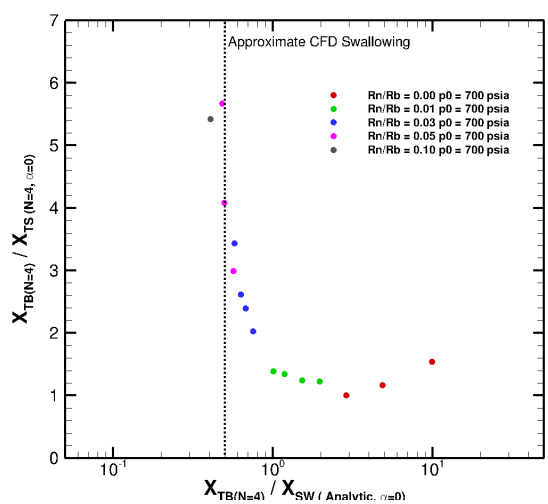

Figure 13. Swallowing Distance vs Predicted Transition

Experimentally, there are cases where transition to turbulence occurs well within the entropy-swallowing

DISTRIBUTION STATEMENT A: Approved for public release;
Distribution is unlimited.

Downloaded by AFRL D'Azzo Wright-Patterson on June 19, 2017 | http://arc.aiaa.org | DOI: 10.2514/6.2017-0764

distances. Both first- and second-mode N-Factor levels at these locations are well below what would be expected to lead to transition from modal growth. It is hoped that frequency and wave angle information from the upcoming experimental series will help to shed some light onto this issue.

VII. Conclusions

Computational simulations of seven-degree half-angle cones have been completed and analyzed with regards to second mode instabilities. It has been shown that computationally derived entropy swallowing distances confirm the trends shown by analytical methods, and both are a good figure of merit when considering bluntness effects on transition. Stability results suggest that the hypothesis that bluntness effects for the most part delay amplification of instabilities rather than increase the critical amplitude is correct. When the experimentally observed transition front is within the entropy swallowing distance, stability results suggest that second mode is not the responsible mode, and some other mechanism is likely causing transition to turbulence.

VIII. Future Work

At the time of writing, the experiential series after which these computations are modeled is underway as of January 2017. Comparison with the expected experimental data, in particular the observed frequencies in the boundary layer, are hoped to clarify what transition phenomena are present on the cone.

Future computational work has been started include characterization of the crossflow instabilities known to be present on the shoulders of yawed cones. A second area of investigation is the effect of wall-temperature ratios on the overall transition pattern.

IX. Acknowledgments

The authors would like to thank Dr. Chau-Lyan Chang for the use of the LASTRAC and LASTRAC3D stability suite, as well as for lending expertise in troubleshooting its use. Computational resources were provided and supported by the DoD HPCMP. Drs. Nicholas Bisek, Ryan Gosse, and Timothy Leger (AFRL/RQHF) provided support and expertise in the use of DoD HPC Systems, as well as the US3D flow solver. Drs. Matthew Borg, Joseph Jewell, and King-Yiu Lam provided many useful discussions on issues of boundary-layer stability and of hypersonic flow in general. Joe Jewell also provided experimental data and provided data and analysis related to previous studies.

References

[1]Alba, C. R., Johnson, H. B., Bartkowicz, M. D., Candler, G. V., and Berger, K. T., "Boundary-Layer Stability Calculations for the HIFiRE-1 Transition Experiment," *Journal of Spacecraft and Rockets*, Vol. 45, No. 6, 2008, pp. 1125–1133.

[2]Stetson, K. F., "Mach 6 Experiments of Transition on a Cone at Angle of Attack," *Journal of Spacecraft*, Vol. 19, No. 5, 1982, pp. 397–403.

[3]Stetson, K. F. and Rushton, G. H., "Shock Tunnel Investigation of Boundary-Layer Transition at M=5.5," *AIAA Journal*, Vol. 5, No. 5, 1967, pp. 899–906.

[4]DiCristina, V., "Mach 6 Experiments of Transition on a Cone at Angle of Attack," *AIAA Journal*, Vol. 8, 1970, pp. 852–856.

[5]Holden, M. S., Bower, D. R., and Chadwick, K. M., "Measurements of Boundary Layer Transition on Cones at Angle of Attack for Mach Numbers from 11 to 13," *AIAA-95-2294*, 1995.

[6]Wadhams, T. P., MacLean, M. G., Holden, M. S., and Mundy, E., "Pre-Flight Ground Testing of the Full-Scale FRESH FX-1 at Fully Duplicated Flight Conditions," *AIAA-2007-4488*, 2007.

[7]Wadhams, T. P., Mundy, E., MacLean, M. G., and Holden, M. S., "Ground Test Studies of the HIFiRE-1 Transition Experiment Part 1: Experimental Results," *Journal of Spacecraft and Rockets*, Vol. 6, No. 45, 2008, pp. 1134–1148.

[8]Wadhams, T. P., MacLean, M. G., and Holden, M. S., "Recent Experimental Studies of High Speed Boundary Layer Transition in LENS Facilities to Further the Development of Predictive Tools for Boundary Layer Transition in Flight," *AIAA-2012-0470*, 2012.

[9]Berger, K. T., Greene, F. A., and Kimmel, R. L., "Aerothermodynamic Testing and Boundary Layer Trip Sizing of the HIFiRE Flight 1 Vehicle," *AIAA-2008-640*, 2008.

[10]Juliano, T. J., Kimmel, R. L., Willems, S., Gülhan, A., and Schneider, S. P., "HIFiRE-1 Surface Pressure Fluctuations from High Reynolds, High Angle Ground Test," *AIAA-2014-4029*, 2014.

[11]Lei, J. and Zhong, X., "Linear Stability Analysis of Nose Bluntness Effects on Hypersonic Boundary Layer Transition,"

Downloaded by AFRL D'Azzo Wright-Patterson on June 19, 2017 | http://arc.aiaa.org | DOI: 10.2514/6.2017-0764

DISTRIBUTION STATEMENT A: Approved for public release;
Distribution is unlimited.

Journal of Spacecraft and Rockets, Vol. 49, No. 1, 2012.

[12]Jewell, J. S. and Kimmel, R. L., "Boundary Layer Stability Analysis for Stetson's Mach 6 Blunt Cone Experiments," *AIAA-2016-0598*, 2016.

[13]Fiore, A. W. and Law, C. H., "Aerodynamic Calibrations of the Aerospace Research Laboratories M = 6 High Reynolds Number Facility," *ARL-TR-75-0028*, 1975.

[14]Candler, G. V., Johnson, H. B., Nompelis, I., Subbareddy, P. K., Drayna, T. W., Gidzak, V., and Barnhardt, M. D., "Development of the US3D Code for Advanced Compressible and Reacting Flow Simulations," *AIAA-2015-1893*, 2015.

[15]Chang, C.-L., "The Langley Stability and Transition Analysis Code (LASTRAC): LST, Linear & Nonlinear PSE for 2-D, Axisymmetric, and Infinite Swept Wing Boundary Layers," *AIAA-2003-0974*, 2003.

[16]Chang, C.-L., *The Langley Stability and Transition Analysis Code (LASTRAC) Version 1.2 User Manual*, June 2004.

[17]Chang, C.-L., "LASTRAC 3D: Transition Prediction in 3-D Boundary Layers," *AIAA-2004-2542*, 2004.

[18]Perez, E., Reed, H. L., and Kuehl, J. J., "Instabilites on a Hypersonic Yawed Cone," *AIAA-2013-2879*, 2013.

[19]Dinzl, D. J. and Candler, G. V., "Analysis of Crossflow Instability on HIFiRE-5 using Direct Numerical Simulation," *AIAA-2015-0279*, 2015.

[20]Traugott, S. C., "Some Features of Supersonic and Hypersonic Flow About Blunted Cones," *Journal of Aerospace Sciences*, Vol. 29, No. 4, 1962, pp. 389–399.

[21]Cleary, J. W., "An Experimental and Theoretical Investigation of the Pressure Distribution and Flow Fields of Blunted Cones at Hypersonic Mach Numbers," *NACA TN D-2969*, 1965.

[22]Stetson, K. F., "Nosetip Bluntness Effects on Cone Frustum Boundary Layer Transition in Hypersonic Flow," *AIAA-83-1763*, 1983.

[23]Zakkay, V. and Krause, E., "Boundary Conditions at the Outer Edge of the Boundary Layer on Blunted Conical Bodies," *AIAA Journal*, Vol. 1, No. 7, 1963, pp. 1671–1672.

[24]Rotta, N. R., "Effects of Nose Bluntness on the Boundary Layer Characteristics of Conical Bodies at Hypersonic Speeds," *NYU-AA-66-66*, 1966.

[25]Klaimon, J. H., "Bow Shock Correlation for Slightly Blunted Cones," *AIAA Journal*, Vol. 1, No. 2, 1963, pp. 490–491.

[26]Billig, F. S., "Shock-Wave Shapes around Spherical- and Cylindrical-Nosed Bodies," *Journal of Spacecraft*, Vol. 4, No. 6, 1967, pp. 822–823.

[27]Juliano, T. J., Kimmel, R. L., Willems, S., Gülhan, A., and Wagnild, R. M., "HIFiRE-1 Boundary-Layer Transition: Ground Test Results and Stability Analysis," *AIAA-2015-1736*, 2015.

[28]Marineau, E. C., Moraru, G., Lewis, D. R., Norris, J. D., Lafferty, J. F., Wagnild, R. M., and Smith, J. A., "Mach 10 Boundary-Layer Transition Experiments on Sharp and Blunted Cones," *AIAA-2014-3108*, 2014.

[29]Jewell, J. S., *Boundary-Layer Transition on a Slender Cone in Hypervelocity Flow with Real Gas Effects*, Ph.D. thesis, California Institute of Technology, May 2015.

Downloaded by AFRL D'Azzo Wright-Patterson on June 19, 2017 | http://arc.aiaa.org | DOI: 10.2514/6.2017-0764

DISTRIBUTION STATEMENT A: Approved for public release;
Distribution is unlimited.